Materials Research Bulletin 187 (2025) 113385

Contents lists available at ScienceDirect

Materials Research Bulletin

journal homepage: www.elsevier.com/locate/matresbu

Research Papers

Exploring the magnetic percolation threshold in the improper ferroelectric $Sr_3Sn_2O_7$ upon Cr and Fe-doping

J. Blasco [a,b,*], V. Cuartero [a,c], S. Lafuerza [a,b], D. Gracia [a,b], J.A. Rodríguez-Velamazán [d], I. Puente-Orench [a,d], G. Subías [a,b]

[a] Instituto de Nanociencia y Materiales de Aragón (INMA), CSIC-Universidad de Zaragoza, 50009 Zaragoza, Spain
[b] Departamento de Física de la Materia Condensada, Universidad de Zaragoza, C/ Pedro Cerbuna 12, 50009 Zaragoza, Spain
[c] Departamento de Ciencia y Tecnología de Materiales y Fluidos, EINA, Universidad de Zaragoza, C/María de Luna 3, 50018 Zaragoza, Spain
[d] Institut Laue-Langevin, Boîte Postale 156, 38042 Grenoble, France

ARTICLE INFO

Keywords:
Complex oxides
Ruddlesden-Popper phase
Magnetic properties
Multiferroics
Electrical properties
Spin glass

ABSTRACT

We examine the effect of Fe and Cr substitutions at the Sn site on the magnetic properties of the hybrid improper ferroelectric $Sr_3Sn_2O_7$. Upon co-doping with La to preserve the electric charge balance in the unit cell, the $Sr_{3-x}La_xSn_{2-x}Cr_xO_7$, $Sr_{3-x}La_xSn_{2-x}Fe_xO_7$ and $Sr_2LaSnFe_{1-y}Cr_yO_7$ series can be obtained as single phases up to $x = 1$ and for all y values. The unit cell volume is isotropically reduced with doping, so that the orthorhombic structure is preserved. However, these substitutions strongly destabilize the ferroelectric order by decreasing the transition temperature, T_{FE}, below room temperature for $x \geq 0.25$. La/Cr co-doping is unable to induce long-range magnetic and compositions from this series behave as conventional paramagnetic compounds; although for high doping concentration ($x \geq 0.5$), the significant deviations from the Curie law at low temperatures suggest the onset of antiferromagnetic correlations. In the case of La/Fe co-doping, all samples show strong antiferromagnetic correlations, but a spin glass-like behavior is observed for $x \approx 1$ compounds. Finally, no long-range magnetic ordering is observed in La/Cr-Fe co-doped samples, but at the same time an increase in spontaneous magnetization is seen at low temperature, which is associated with the presence of competitive magnetic interactions, in particular the Fe-O-Cr superexchange ferromagnetic interaction. The lack of long-range magnetic order in the investigated series of Cr/Fe-doped $Sr_3Sn_2O_7$, indicates that the critical concentration of magnetic atoms necessary to overcome the magnetic percolation threshold exceeds the 50 % in magnetic cations in these bilayered Ruddlesden-Popper perovskites.

1. Introduction

Recent studies have proved that $Sr_3Sn_2O_7$ is an improper ferroelectric with switchable electric polarization at room temperature with a large coercive field [1,2]. In addition, it can be grown as single crystal using the floating zone method and shows ferroelectricity with a smaller coercivity compared to the ceramic specimens [3]. $Sr_3Sn_2O_7$ is a member of Ruddlesden-Popper (RP) series, $A_{n+1}B_nO_{3n+1}$ (A=Sr; B=Sn) with $n = 2$. Its crystal structure consists of alternating perovskite bilayers (ABO_3) and rock-salt-like layers (AO) along the c-axis (see Fig. 1). The undistorted ideal structure is tetragonal with space group $I4/mmm$ but the small size of Sr^{2+} produces structural strain that is relieved by cooperative rotations and tilts of the SnO_6 octahedra, which reduces the symmetry of the unit cell to orthorhombic (space group $A2_1am$). This is the basis for the hybrid improper ferroelectric (HIF) mechanism where two main non-polar distortions (the abovementioned rotation and tilt of SnO_6 octahedra) are coupled to favor the condensation of a secondary ferroelectric distortion [4–6]. In this way, $Sr_3Sn_2O_7$ can be classified as a geometric improper ferroelectric compound. The discovery of new mechanisms for ferroelectricity, such as the HIF in complex perovskite-based layered structure systems, paves the way for the search of new multiferroic materials at room temperature [7], since in principle this mechanism is compatible with the presence of magnetic cations at the B site of the perovskite layers. Following this strategy, the non-magnetic cation Sn^{4+} in $Sr_3Sn_2O_7$ is replaced with magnetic cations trying to reach the magnetic percolation. This percolation is reached when the concentration of magnetic atoms exceeds a critical threshold, which triggers a phase transition from a disordered to a long-range

* Corresponding author.
E-mail address: jbc@unizar.es (J. Blasco).

https://doi.org/10.1016/j.materresbull.2025.113385
Received 17 December 2024; Received in revised form 12 February 2025; Accepted 18 February 2025
Available online 19 February 2025

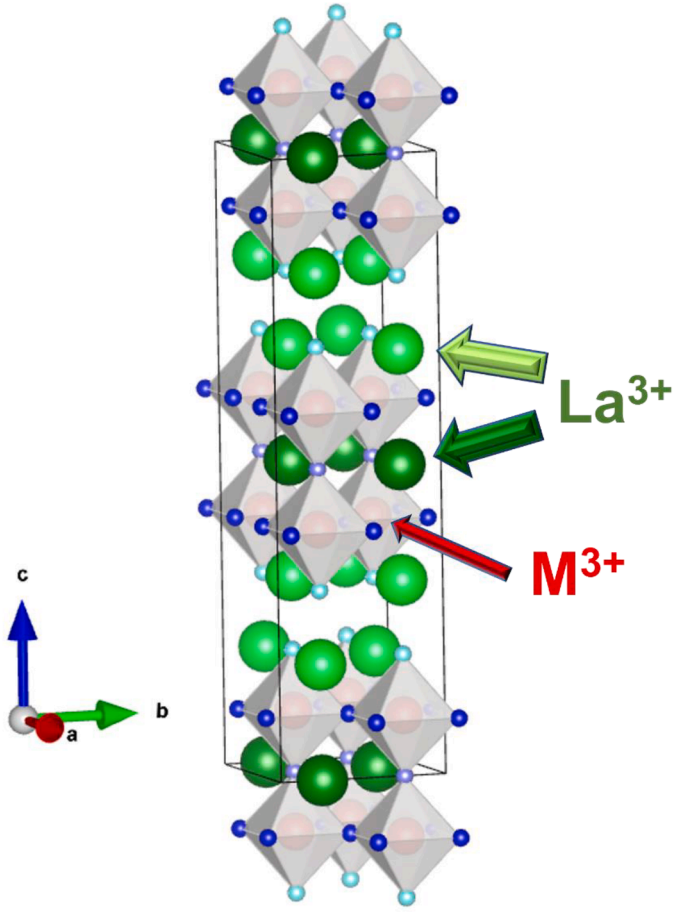

Fig. 1. Orthorhombic crystal structure of $Sr_3Sn_2O_7$ and type of co-doping to preserve the electrical charge balance. Big green, intermediate red and small blue balls stand for Sr, Sn and O atoms, respectively.

magnetic ordered ground state. The critical concentration of magnetic atoms depends on the type of perovskite structure, the nature of the magnetic atoms, and the temperature of the system. Regarding the crystal structure, there are important differences between a simple perovskite and a RP phase with $n = 1$, A_2BO_4. In the first case, each BO_6 octahedron is linked with 6 neighboring octahedra establishing a three-dimensional (3D) lattice. For A_2BO_4, each BO_6 octahedron is connected with 4 neighboring ones forming two-dimensional (2D) layers which are kept separated by the AO rock-salt layer. Following pioneering studies on the critical percolation for 2D and 3D lattices [8], some experimental studies determined the critical concentration of magnetic atoms at $T = 0$ K, x_c, in both types of structures for diluted Heisenberg antiferromagnets [9]. Values of x_c= 0.31 and 0.59 are obtained for a simple perovskite and a 2D-RP phase, respectively. These values agree with the ones expected from numerical calculations [8,9]. Further studies on 2D-RP phases with antiferromagnetic (AFM) order reveal that Heisenberg magnets show a higher T_N decrease rate than 2D Ising magnets in the low concentration range of non-magnetic ions [10]. However, both types of magnets show similar x_c values in most cases [10]. In the case of a RP phase with perovskite bilayers like $Sr_3Sn_2O_7$, each SnO_6 octahedron is linked with 5 neighboring octahedra so that an intermediate x_c-value between the two previous cases can be expected. In all instances, these numbers should be taken as a first approximation because the nature of the magnetic cations and the magnetic interactions also play a role. Very few studies have been devoted to the effects of magnetic dilution on $A_3B_2O_7$ RP phases. For instance, in the particular case of manganites dominated by the competing interactions of Mn^{3+} and Mn^{4+}, both $(La,Ca)MnO_3$ and $(La,Ca)_3Mn_2O_7$ show long-range magnetic order with similar T_N for the same doping degree, whereas $(La,Ca)_2MnO_4$ presents a spin glass behavior [11]. Another study on $LaSr_2Mn_{2-x}Al_xO_7$ reported a T_N reduction according to a 2D Heisenberg system for $x \leq 0.2$, but x_c was not determined [12].

In the present work we explore the magnetic percolation threshold in the HIF $Sr_3Sn_2O_7$ by replacing Sn^{4+} with magnetic Fe^{3+} and/or Cr^{3+} cations, that are intended to induce different magnetic interactions and orderings. According to Goodenough-Kanamori rules [13,14], the 180º magnetic superexchange interactions should be AFM for Fe^{3+}-O-Fe^{3+} and Cr^{3+}-O-Cr^{3+} but ferromagnetic (FM) for Fe^{3+}-O-Cr^{3+}. The experimental results obtained in simple perovskites support these rules as strong AFM is reported for $LaFeO_3$ (T_N≈740 K) [15] and more moderate for $LaCrO_3$ (T_N≈283 K) [16]. However, complex magnetic interactions are observed in $LaFe_{0.5}Cr_{0.5}O_3$, giving rise to controversial results in the literature. Neutron diffraction studies determined a canted AFM ordering with a FM component at T_N≈265 K for this compound [17], but a ferrimagnetic behavior is also observed in the magnetization measurements with a strong magnetic irreversibility. The occurrence of ferromagnetic clusters around room temperature followed by a compensation temperature at $T \approx 190$ K has also been reported, which clearly indicates the presence of competitive magnetic interactions in this compound [18,19]. The diverse electronic configurations of Fe^{3+} ($3d^5$ and $S = 5/2$) and Cr^{3+} ($3d^3$ and $S = 3/2$) may also lead to different magnetic behaviors: Fe^{3+} is a quite isotropic cation while Cr^{3+} may exhibit a net orbital angular moment contribution. Nonetheless, Cr^{3+}spin can usually point in any direction, reflecting isotropic spin-spin interactions according to Heisenberg model [20]. A similar behavior is expected for Fe^{3+}, although some studies reported that this cation may behave as an Ising magnetic cation in anisotropic structures, so that their magnetic interactions are primarily restricted along one axis [21].

The magnetic doping species at Sn^{4+} site are trivalent, so the electric charge balance of the unit cell is preserved by the simultaneous substitution of Sr^{2+} for La^{3+}, which can be placed at any of the two available A-sites in the crystal structure (Fig. 1). This type of co-doping strategy in two positions of layered structures has already been successfully carried out in related complex oxide systems [22]. In particular, the effect of replacing strontium with other alkaline earth metals (A= Ba, Ca) in $Sr_2Sn_2O_7$ reveals that the ferroelectric transition temperature (from here on, denoted as T_{FE} to differentiate it from the ferromagnetic transition temperature Tc) increases as the average size of the A atom decreases [23,24]. This effect suggests a relationship between T_{FE} and the tolerance factor (t-factor) of the perovskite layers, defined as $t=(r_A+r_O)/\sqrt{2}(r_B-r_O)$, where r_A, r_B and r_O represent the ionic radii of A-site cation, B-site cation, and oxygen anion, respectively. A decrease of t-factor favors the tilts and rotations of the BO_6 octahedra that lead to the appearance of improper ferroelectricity. All these distortions are active in $LaFeO_3$ or $LaCrO_3$, which aligns with our co-doping strategy. In this work we present a thorough structural, magnetic and electric characterization for samples doped with a single magnetic cation, $Sr_{3-x}La_xSn_{2-x}Cr_xO_7$ and $Sr_{3-x}La_xSn_{2-x}Fe_xO_7$, and with two magnetic atoms: $Sr_2LaSnFe_{1-y}Cr_yO_7$.

2. Experimental

Polycrystalline samples of $Sr_{3-x}La_xSn_{2-x}Cr_xO_7$, $Sr_{3-x}La_xSn_{2-x}Fe_xO_7$, and $Sr_2LaSnFe_{1-y}Cr_yO_7$ ($0 \leq x, y \leq 1$) were synthesized by solid state reaction in three steps as reported elsewhere [25]. Stoichiometric amounts of SnO_2, $SrCO_3$, La_2O_3, Cr_2O_3 and Fe_2O_3 (nominal purities not <99.9 % in wt.) were mixed, ground and heated at 1273 K for 15 h in air. The resulting powder was reground, pressed into pellets and sintered at 1573 K for 24 h. Thus, the pellets were reground, repressed and sintered at 1673 K for another 24 h. The heating and cooling ramps were 5 K/min in all steps. The samples were characterized by X-ray powder diffraction (XRD) using a Rigaku D-system using Cu $K\alpha_{1,2}$ wavelengths. Neutron powder diffraction (NPD) measurements were performed at the high-flux reactor of the ILL (Grenoble, France) using the high-intensity

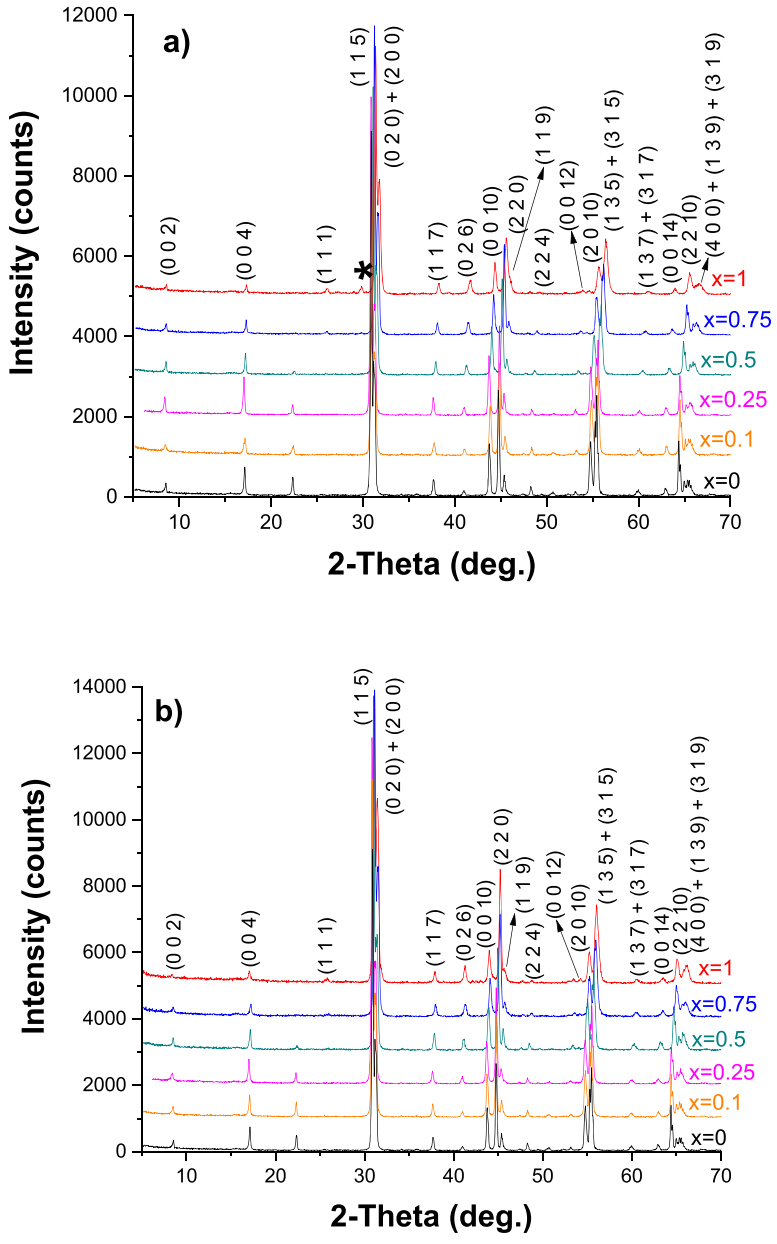

Fig. 2. XRD patterns of $Sr_{3-x}La_xSn_{2-x}Cr_xO_7$ (a) and $Sr_{3-x}La_xSn_{2-x}Fe_xO_7$ (b) samples including the indexation of the main diffraction peaks. The patterns are shifted up for the sake of comparison. The asterisk indicates the main impurity peak observed in $Sr_2LaSnCrO_7$.

powder diffractometer D1B with a detector angular range coverage $2^o \leq 2\theta \leq 128^o$, which is especially suited for determination of magnetic orderings. A wavelength of $\lambda \approx 2.52$ Å was used in a temperature range between 2 K and 150 K. Rietveld analysis of XRD patterns were performed with the Fullprof program [26]. The schematic illustrations of the crystal structures were obtained with the VESTA program [27]. The chemical composition of the samples was evaluated by using the wavelength dispersive X-ray fluorescence spectrometry technique (advant'XP+ model manufactured by ARL). The Sr:Sn:B ratio agreed with the nominal one for all samples.

Magnetic measurements were carried out between 5 and 400 K by using a commercial superconducting quantum interference device (SQUID) magnetometer from Quantum Design. The measurements were performed warming the sample after zero-field cooling at an external magnetic field of 1 kOe. Isothermal magnetization measurements at selected temperatures between 5 and 250 K were performed for externals fields between −50 and 50 kOe. The relative dielectric permittivity was derived from measurements with an impedance analyzer (Wayne Kerr Electronics 6500B), applying sinusoidal excitations of 1 V amplitude at 900 kHz. Temperature dependent measurements were conducted in homemade sample insert in either a tubular furnace (upon heating above room temperature) or an Oxford Instruments cryostat (from 120 K up to 400 K), with 1 K/minute heating ramps. The polarization versus electric field (*P-E*) hysteresis loops were collected at room temperature in silicon oil, using a 500 V-built-in ferroelectric tester (Precision Premier II, Radiant Technologies) jointly with a high voltage amplifier (610E, Trek). Excitation signals with frequency of either 100 or 250 Hz and maximum electric (*E*) field amplitude of 125 kV/cm were applied. X-ray absorption spectra (XAS) of the Fe $L_{2,3}$ edge (700–730 eV) of $Sr_2LaSnFeO_7$ was measured at room temperature by total electron yield detection at the BL29 BOREAS beamline at ALBA synchrotron [28].

Table 1
Refined lattice parameters for $Sr_{3-x}La_xSn_{2-x}Cr_xO_7$, $Sr_{3-x}La_xSn_{2-x}Fe_xO_7$ and $Sr_2LaSnFe_{1-y}Cr_yO_7$ compounds using the orthorhombic cell with space group $A2_1am$ (or *Amam*). Numbers in parentheses indicate the errors in the last significant digits.

Sample	a (Å)	b (Å)	c (Å)	Vol. (Å^3)
$Sr_3Sn_2O_7$	5.7066 (1)	5.7352 (1)	20.6649(1)	676.33(1)
$Sr_{3-x}La_xSn_{2-x}Cr_xO_7$ series				
$Sr_{2.9}La_{0.1}Sn_{1.9}Cr_{0.1}O_7$	5.6985 (1)	5.7269 (1)	20.6320(2)	673.32(1)
$Sr_{2.75}La_{0.25}Sn_{1.75}Cr_{0.25}O_7$	5.6765 (3)	5.7039 (3)	20.6117(9)	667.38(5)
$Sr_{2.5}La_{0.5}Sn_{1.5}Cr_{0.5}O_7$	5.6549 (4)	5.6821 (4)	20.5278 (13)	659.59(7)
$Sr_{2.25}La_{0.75}Sn_{1.25}Cr_{0.75}O_7$	5.6289 (3)	5.6543 (3)	20.4336(7)	650.34(5)
$Sr_2LaSnCrO_7$	5.6037 (7)	5.6306 (7)	20.3723 (14)	642.80 (14)
$Sr_{3-x}La_xSn_{2-x}Fe_xO_7$ series				
$Sr_{2.9}La_{0.1}Sn_{1.9}Fe_{0.1}O_7$	5.7016 (1)	5.7296 (1)	20.6365(2)	674.15(1)
$Sr_{2.75}La_{0.25}Sn_{1.75}Fe_{0.25}O_7$	5.6854 (3)	5.7135 (3)	20.6175 (11)	669.73(6)
$Sr_{2.5}La_{0.5}Sn_{1.5}Fe_{0.5}O_7$	5.6706 (3)	5.7031 (3)	20.5625 (12)	665.00(7)
$Sr_{2.25}La_{0.75}Sn_{1.25}Fe_{0.75}O_7$	5.6497 (5)	5.6763 (5)	20.4915(9)	657.15(9)
$Sr_2LaSnFeO_7$	5.6265 (6)	5.6528 (6)	20.4552 (13)	650.59 (13)
$Sr_2LaSnFe_{1-y}Cr_yO_7$ series				
$Sr_2LaSnFe_{2/3}Cr_{1/3}O_7$	5.6188 (4)	5.6466 (4)	20.4166(8)	647.75(8)
$Sr_2LaSnFe_{1/2}Cr_{1/2}O_7$	5.6140 (4)	5.6435 (4)	20.4111(7)	646.67(7)
$Sr_2LaSnFe_{1/3}Cr_{2/3}O_7$	5.6068 (3)	5.6356 (3)	20.3849(7)	644.12(7)

3. Results and discussion

3.1. Structural effects of co-doping in the HIF behavior of $Sr_3Sn_2O_7$

Fig. 2(a) and (b) show the XRD patterns of the $Sr_{3-x}La_xSn_{2-x}Cr_xO_7$ and $Sr_{3-x}La_xSn_{2-x}Fe_xO_7$ ($x = 0$, 0.1, 0.25, 0.5, 0.75 and 1) series, respectively. All samples are single phase, except for the $x = 1$ Cr-doped compound, that exhibits a minor pyrochlore impurity (0.8(1) % in wt. estimated from the Rietveld refinement).

Both the $Sr_{3-x}La_xSn_{2-x}Cr_xO_7$ and $Sr_{3-x}La_xSn_{2-x}Fe_xO_7$ series can be refined to the polar $A2_1am$ structure, identical to that of the parent compound $Sr_3Sn_2O_7$ [1–3]. The refined lattice parameters are summarized in Table 1. The volume of the unit cell decreases linearly as the degree of co-doping in the series increases, according to the different tabulated ionic radii [29]: $r^{3+}_{La} < r^{2+}_{Sr}$ and $r^{3+}_{Cr}(r^{3+}_{Fe}) < r^{4+}_{Sn}$ with r^{3+}_{La}, r^{2+}_{Sr}, r^{3+}_{Cr}, r^{3+}_{Fe} r^{4+}_{Sn}. Also, the volume reduction is less pronounced in Fe-doped samples, as $r^{3+}_{Fe} > r^{3+}_{Cr}$ (0.645 and 0.615 Å^3, respectively). The contraction of the unit cell volume is quite isotropic, as all lattice parameters are equally reduced, being −0.21 Å^3/x and −0.29 Å^3/x for the Fe- and Cr-based series, respectively. (see Table 1). Single phases of the $Sr_2LaSnFe_{1-y}Cr_yO_7$ series have also been obtained with $y = 1/3$, 1/2 and 2/3. The refined lattice parameters are also listed in Table 1 and they can be compared with $Sr_2LaSnFeO_7$ ($y = 0$) and $Sr_2LaSnCrO_7$ ($y = 1$). These parameters continuously decrease as the *y*-value does reflecting the fact that $r^{3+}_{Fe} > r^{3+}_{Cr}$. The lattice evolution is continuous between the two limits of this series.

Given the absence of impurities in $Sr_2LaFeSnO_7$, we decided to increase the degree of Fe substitution. For samples with $x > 1$, secondary phases of simple perovskite and 2D-RP AB_2O_4 phases appear in the XRD patterns, while at $x = 1.25$, these become the majority phases (see supplementary information). It seems that for this concentration range the equilibrium $A_3B_2O_7 \leftrightarrows ABO_3 + A_2BO_4$ (*A*=La, Sr; *B*=Fe, Sn) is shifted to the right side.

Our recent study on the electrical properties of the $Sr_{3-x}La_xSn_{2-x}M_xO_7$ ($x = 0$ and 0.1; M=Cr, Fe or Mn) compounds revealed that this type of aliovalent co-doping weakens the ferroelectric ordering, which is evidenced by a significant decrease in the T_{FE} even for these small doping concentrations [25]. $Sr_3Sn_2O_7$ is white. However, the doped samples are colored and the color evolves from a light yellow (Fe) or coral (Cr) for $x = 0.1$ through a dark yellow (Fe) or brown (Cr) for $x = 0.5$ until reaching a very dark brown for both doped samples with $x = 1$. This darkening of the samples upon doping reflects an increase in structural defects which is also reflected in the electrical properties. Samples become more conductive and space charge polarization effects due to the presence of mobile ions is the largest contribution to the dielectric permittivity measured at low frequencies, hiding the anomaly produced in the ferroelectric transition. At high frequencies the dipole ordering becomes the most important contribution to the dielectric permittivity and the samples can be compared, regardless of the differences in electrical conduction. Fig. 3 (top panel) compares the real part of the relative electrical permittivity of the $Sr_{3-x}La_xSn_{2-x}Fe_xO_7$ ($x \leq 0.5$) samples at a frequency of 900 kHz in a heating ramp. The ferroelectric transition of $Sr_3Sn_2O_7$ is characterized by an anomaly with a peak at 409 K whose position does not depend on the frequency of the electric field. This temperature agrees with previous reports [2,23,25] and it was identified as a first-order transition [30]. As the Fe content in the sample increases, the anomaly widens and appears at lower temperatures confirming that co-doping weakens the ferroelectric ordering. We note that the shape of the anomaly is frequency independent for $x = 0.1$, revealing a conventional ferroelectric transition like the undoped compound. In the case of the sample with $x \geq 0.25$, the frequency range with dominant electronic contribution is very limited and thus prevents characterizing the occurrence of a relaxor behavior in the wide transition observed in these samples. Fig. 3 (bottom panel) compares the *P-E* loops for $Sr_{2.9}La_{0.1}Sn_{1.9}Fe_{0.1}O_7$ and $Sr_{2.75}La_{0.25}Sn_{1.75}Fe_{0.25}O_7$ samples that were measured applying the standard bipolar triangular voltage pulse (main panel) and the remanent hysteresis measurement protocols based on the *PUND* method [31] (inset). The comparison is made at the highest *E* field value allowed by the second sample. Clearly, the leakage current increases as does the Fe content in the sample, producing more open loops. A well-developed hysteresis loop is observed in the remanent hysteresis measurement for the $Sr_{2.9}La_{0.1}Sn_{1.9}Fe_{0.1}O_7$ compound and the J-*E* curve shows peaks around the coercive field (see supplementary information) confirming an intrinsic remanent polarization at room temperature for this composition. However, the same measurement in the $Sr_{2.75}La_{0.25}Sn_{1.75}Fe_{0.25}O_7$ sample shows a negligible remanent polarization within experimental error, around ten times smaller than the previous sample. These measurements were not possible for samples with higher Fe concentration due to their high electrical conductivity at room temperature.

Therefore, samples with $x \geq 0.25$ are no longer considered as ferroelectric above room temperature, even though the orthorhombic distortion is preserved throughout the series. This indicates that the real space group for samples with a high degree of Sn substitution is centrosymmetric. These patterns can be refined using the *Amam* space group, instead of the polar $A2_1am$ at room temperature. We note here that, differentiating between these space groups by conventional XRD is very hard because they have the same allowed reflections. In related systems, it has been suggested that the strong competition between the rotation of the BO_6 octahedra (causing the HIF mechanism) and an atomic rumpling at the rock salt-perovskite interface producing a deformation of the BO_6 octahedra, can effectively suppress the HIF mechanism [32]. Finally, another factor to be considered is that disorder at the B-sites also affects the BO_6 rotations, weakening the HIF mechanism.

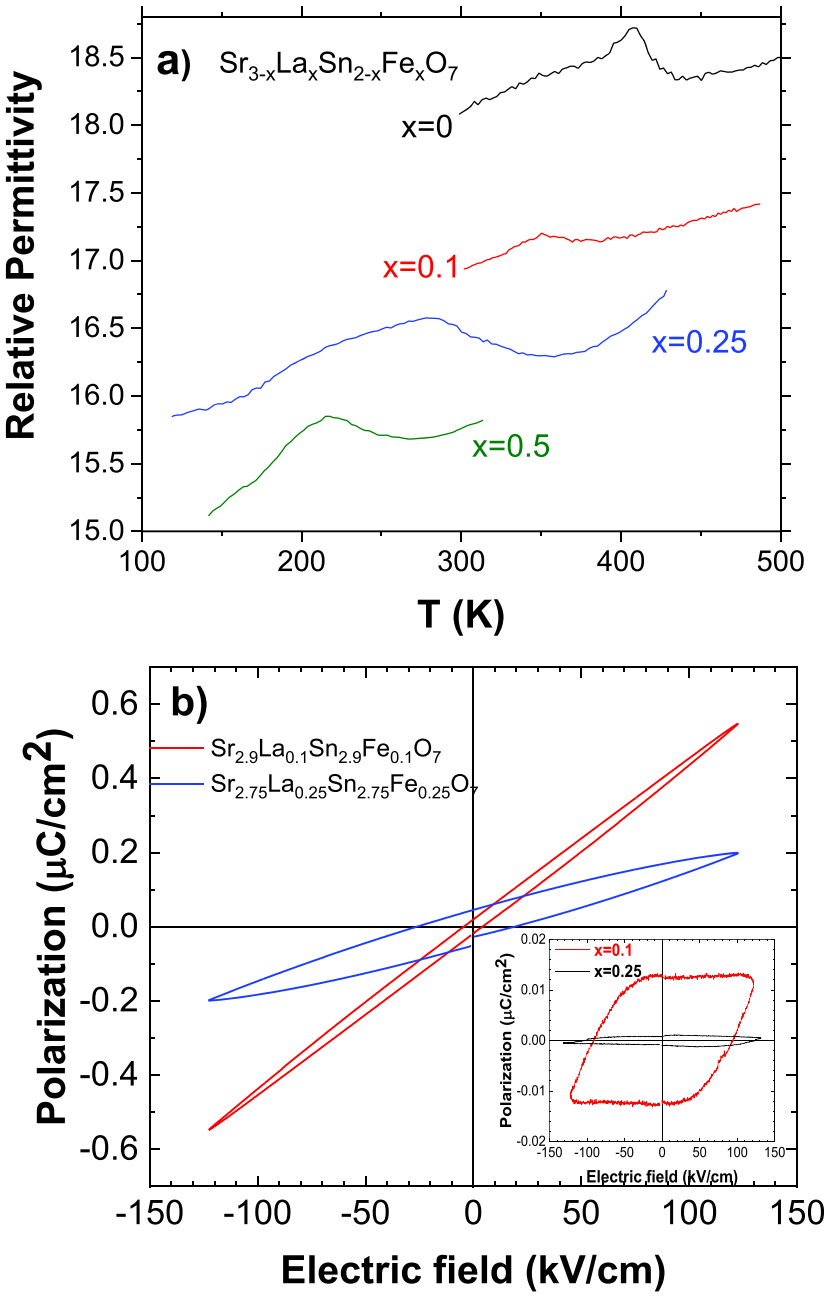

Fig. 3. (a) The real component of the relative dielectric permittivity for $Sr_3Sn_2O_7$, and doped $Sr_{3-x}La_xSn_{2-x}Fe_xO_7$ ($x \leq 0.5$) samples at 900 kHz; (b) Polarization hysteresis *P-E* loops for $Sr_{2.9}La_{0.1}Sn_{1.9}Fe_{0.1}O_7$ and $Sr_{2.9}La_{0.25}Sn_{1.75}Fe_{0.25}O_7$ measured at room temperature and at 100 Hz. Inset: Remanent hysteresis loops for the same samples measured at room temperature and at 250 Hz.

3.2. Evolution of the magnetic properties upon Cr and/or Fe doping

3.2.1. $Sr_{3-x}La_xSn_{2-x}Cr_xO_7$

The temperature dependence of the magnetization, M(T), measured at 1 kOe in the $Sr_{3-x}La_xSn_{2-x}Cr_xO_7$ series exhibits a paramagnetic behavior in the whole temperature range without noticeable irreversibility between zero-field-cooled (ZFC) and field-cooled (FC) conditions. Fig. 4(a) shows the inverse of the magnetic susceptibility vs. temperature curves for this series. All doped samples obey the Curie-Weiss law at high temperatures ($T > 200$ K), showing a deviation at low temperature that suggests a polarization of the magnetic moments. Nonetheless, long-range magnetic ordering is not developed in any of these compounds as will be shown below by the analysis of the neutron diffraction results. Table 2 summarizes the magnetic parameters obtained from the linear fits shown in Fig. 4(a). The Curie constant increases with the content of paramagnetic cations (Cr^{3+}), as expected. Overall, the calculated effective paramagnetic moments (ρ_{eff}) reasonably agree with the theoretical ones considering the spin-only contribution of high spin Cr^{3+}. All these samples have a negative Weiss constant that indicates the presence of AFM correlations in the paramagnetic phase. Furthermore, these correlations increase with the Cr-content, in agreement with the expected interactions from the Goodenough-Kanamori rules [13,14].

The H field dependence of magnetization, M(H), is presented in Fig. 4(b) between +50 kOe and −50 kOe for the $Sr_{3-x}La_xSn_{2-x}Cr_xO_7$ series at 5 K. The lower the concentration of Cr, the easier it is to polarize the samples. This confirms that AFM correlations strengthen with increasing Cr content, although they remain insufficient to establish long-range magnetic order, even for $x = 1$. The inset of Fig. 4 displays the M(H) curves at selected temperatures for the $x = 0.75$ compound as a representative example, since the other samples exhibit a similar

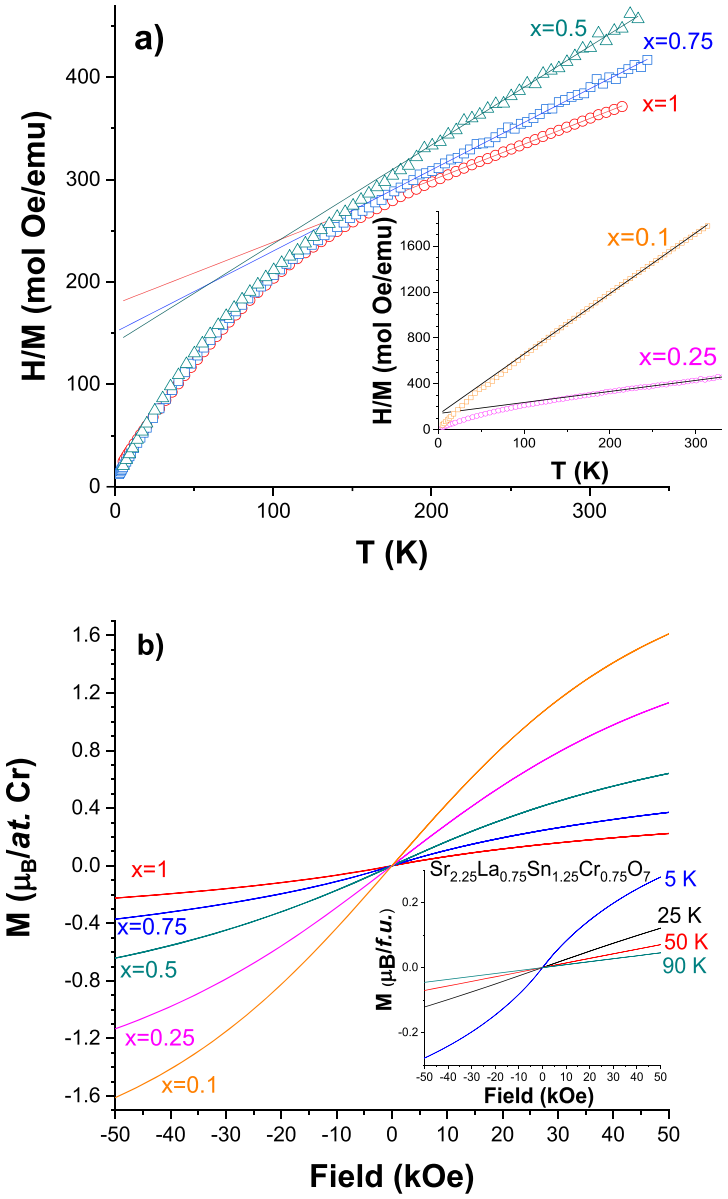

Fig. 4. (a) Inverse magnetization vs. temperature curves for $Sr_{3-x}La_xSn_{2-x}Cr_xO_7$ with x = 0.5, 0.75 and 1. Inset: The same curves for x = 0.1 and 0.25. (b) Magnetization loops for $Sr_{3-x}La_xSn_{2-x}Cr_xO_7$ samples at 5 K. Inset: M(H) measurements at selected temperatures for $Sr_{2.25}La_{0.75}Sn_{1.25}Cr_{0.75}O_7$.

behavior. Except for the lowest temperature, the M(H) curves are nearly straight lines as expected for paramagnetic compounds. At 5 K, they exhibit a nonlinear dependence, similar to that observed for paramagnets following a Langevin function. No remanent magnetization was observed in the M(H) curves, which proves the absence of FM interactions.

3.2.2. $Sr_{3-x}La_xSn_{2-x}Fe_xO_7$

Fig. 5(a) shows the inverse of the magnetic susceptibility vs. temperature for the $Sr_{3-x}La_xSn_{2-x}Fe_xO_7$ series. All samples exhibit paramagnetic behavior between 5 K and room temperature, without any type of anomaly, except for $Sr_2LaSnFeO_7$ (see Fig. 5(b)). The curves show a linear behavior at high temperature and deviate from a Curie-Weiss law at low temperature. The linear range decreases as the sample co-doping increases. While the samples with x = 0.1–0.5 obey Curie's law above 200 K, the sample with x = 1 barely follows it above 250 K and the sample with x = 0.75 shows an intermediate behavior. The magnetic data extracted from the linear fit are also detailed in the Table 2. The Curie constant increases as the Fe content does and all compounds present strong AFM correlations (negative Weiss constants) as expected for Fe^{3+}-O-Fe^{3+} superexchange interactions according to the Goodenough-Kanamori rules [13,14]. The ρ_{eff} values reasonably agree with the theoretical ones for Fe^{3+} cations in the diluted samples ($x \leq$ 0.25), but strong deviations occur as co-doping increases. In fact, the experimental value for $Sr_2LaSnFeO_7$ is close to the spin-only contribution of a high-spin Fe^{2+} although this cation has a significant orbital contribution and its experimental values are around 5.4 μ_B, still closer to the obtained in $Sr_2LaSnFeO_7$ than the expected value for Fe^{3+} [33]. In order to unambiguously determine the oxidation state of Fe in $Sr_2LaSnFeO_7$, XAS measurements were performed at the Fe $L_{2,3}$ edge (see experimental section). The spectral features clearly agree with an Fe^{3+} in octahedral coordination [34] revealing that the oxidation state of Fe^{3+} is preserved throughout the entire series. These results indicate an enhancement of magnetic correlations as the Fe concentration increases, producing deviations of the Curie-Weiss law and a shortening of the temperature range where it can be applied.

Table 2
Curie constant (C), Weiss constant (θ) and experimental effective paramagnetic moments (ρ_{eff}) obtained from the fit to a Curie-Weiss law: $\chi = C/(T-\theta)$. Theoretical effective paramagnetic moments (ρ_{theo}) have been calculated from experimental values for spin-only Cr^{3+} and Fe^{3+}.

Sample	C (emu/K mol)	θ (K)	ρ_{eff} (μ_B/*fu*)	ρ_{theo} (μ_B/*fu*)
$Sr_{3-x}La_xSn_{2-x}Cr_xO_7$ series:				
$Sr_{2.9}La_{0.1}Sn_{1.9}Cr_{0.1}O_7$	0.145	−6	1.08	1.20
$Sr_{2.75}La_{0.25}Sn_{1.75}Cr_{0.25}O_7$	0.42	−44.5	1.83	1.95
$Sr_{2.5}La_{0.5}Sn_{1.5}Cr_{0.5}O_7$	1.04	−146.5	2.88	2.69
$Sr_{2.25}La_{0.75}Sn_{1.25}Cr_{0.75}O_7$	1.26	−190.5	3.18	3.29
$Sr_2LaSnCrO_7$	1.66	−296.5	3.64	3.80
$Sr_{3-x}La_xSn_{2-x}Fe_xO_7$ series:				
$Sr_{2.9}La_{0.1}Sn_{1.9}Fe_{0.1}O_7$	0.355	−33.5	1.69	1.86
$Sr_{2.75}La_{0.25}Sn_{1.75}Fe_{0.25}O_7$	0.93	−57	2.72	2.95
$Sr_{2.5}La_{0.5}Sn_{1.5}Fe_{0.5}O_7$	1.41	−102.1	3.36	4.17
$Sr_{2.25}La_{0.75}Sn_{1.25}Fe_{0.75}O_7$	2.06	−91.5	4.06	5.11
$Sr_2LaSnFeO_7$	2.92	−148.6	4.83	5.90
$Sr_2LaSnFe_{1-y}Cr_yO_7$ series:				
$Sr_2LaSnFe_{2/3}Cr_{1/3}O_7$	2.45	−136.9	4.43	5.27
$Sr_2LaSnFe_{1/2}Cr_{1/2}O_7$	2.36	−123.3	4.35	4.96
$Sr_2LaSnFe_{1/3}Cr_{2/3}O_7$	2.31	−129.6	4.30	4.58

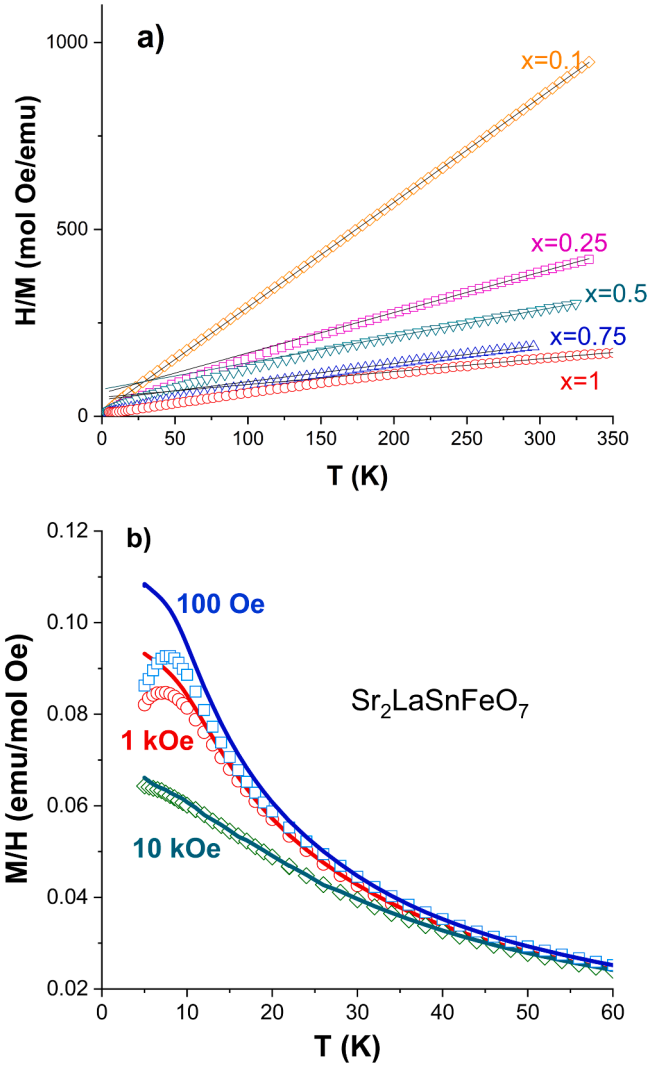

Fig. 5. (a) Inverse magnetization vs. temperature curves for $Sr_{3-x}La_xSn_{2-x}Fe_xO_7$. (b) Magnetization vs. temperature for $Sr_2LaSnFeO_7$ under various applied fields in zero-field-cooling (points) and field-cooling (lines) conditions.

Exceptionally, M(T) curve for $Sr_2LaSnFeO_7$ displays a small magnetic irreversibility at low temperature between zero-field-cooling (ZFC) and field-cooling (FC conditions as can be seen in Fig. 5(b). At low fields, the ZFC curve shows a peak, absent in the FC curve that shows a magnetization that continuously increases with decreasing temperature. The peak temperature decreases with increasing the strength of the magnetic field. Accordingly, at low external magnetic field strengths (100 Oe), the differences between the ZFC and FC curves are more pronounced. However, at high external magnetic field strengths (10 kOe), the difference between the ZFC and FC curves is greatly reduced and almost disappears. Clearly, this field helps to align the spins, reducing disorder and irreversibility. Overall, the observed behavior suggests either the presence of a magnetic system with disorder and frustration, probably a magnetic glassy phase [34,35] or the contribution of domain effects in an ordered system [36]. In order to discern it, neutron powder diffraction patterns for $Sr_2LaSnFeO_7$ have been collected between 2 and 150 K. Fig. 6 compares the measured patterns below and well above the anomaly observed in Fig. 5(b). Neither additional diffraction peaks nor intensity changes in the allowed reflections are observed in the pattern measured at 2 K indicating the absence of long-range magnetic order in this compound.

Fig. 7(a) shows the M(H) loops for all $Sr_{3-x}La_xSn_{2-x}Fe_xO_7$ samples at 5 K normalized to Fe content. The magnitude of magnetization under H decreases as Fe concentration does, as observed in Cr-doped series. However, differently from Cr-doped series, in the case of samples with higher Fe doping, magnetic correlations are evident. Fig. 7(b) focuses on the M(H) curves for $Sr_2LaSnFeO_7$ at selected temperatures: at high temperatures M(H) has linear behavior, typical of a paramagnetic compound; at 5 K remanent magnetization with a small coercive field is observed, as displayed in the inset. This remanent magnetization cannot be ascribed to a canting of magnetic moments in an AFM structure because neutron diffraction has ruled it out. Considering ZFC/FC irreversibility, the most plausible explanation is that structural disorder and competitive magnetic interactions have led to the emergence of a glassy magnetic state. To verify it, we have measured the ac magnetic susceptibility of this compound at different frequencies (see supplementary information). We observe a peak in real component at ≈ 9 K (900 Hz) that slightly shifts to lower temperatures, while increasing its intensity, as the frequency of the magnetic field is decreased. This change in intensity is due to the fact that at higher frequencies, the spins cannot follow the applied magnetic field as quickly, resulting in a diminished response [35]. The imaginary part instead, shows a broad maximum at lower temperatures compared to the real part. In this component, there is an increase in the intensity of the peak at higher frequencies due to the greater dissipation of energy (internal friction) as frequency increases. This dynamic behavior revealed by ac magnetic susceptibility is typical of magnetic spin glasses [35,37]. Then, the magnetic interactions between Fe^{3+} atoms increase with their concentration, leading to short-range magnetic correlations. However, the percolation threshold is not achieved preventing the emergence of a long-range magnetic order.

3.2.3. *$Sr_2LaSnFe_{1-y}Cr_yO_7$*

The $Sr_2LaSnFe_{1-y}Cr_yO_7$ series has been explored with $y = 1/3$, 1/2 and 2/3 with the aim of enhancing Fe-O-Cr FM correlations. These samples also obey the Curie-Weiss law at high temperature and the fitted parameters can be found in Table 2. All samples show negative values of the Weiss constant suggesting the prevalence of AFM correlations in this case as well. The calculated ρ_{eff} have lower values than the expected ones in the Fe-rich samples but are close to their theoretical values in the Cr-rich ones. On cooling, the evolution of magnetization deviates from Curie-Weiss' law, showing a rise at low temperature that is especially strong for samples with $y = 1/3 - 2/3$, as can be seen in Fig. 8(a). Fig. 8 (b) shows the M(T) curves in ZFC and FC conditions for these samples at low temperature. The three samples exhibit magnetic irreversibility, with a peak in the ZFC branch below 5 K that may be related to the

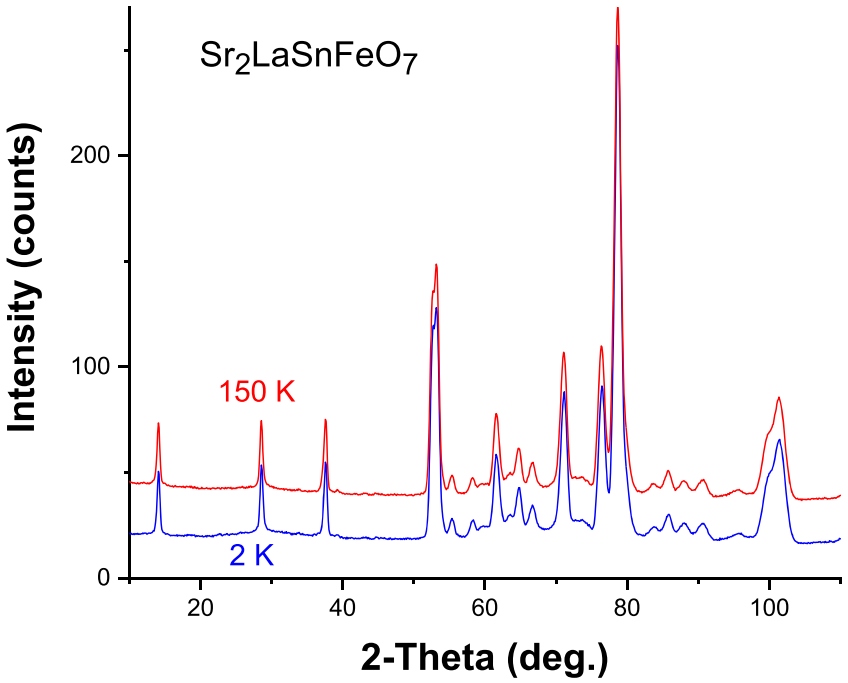

Fig. 6. Comparison of the neutron powder diffraction patterns for $Sr_2LaSnFeO_7$ collected at 2 and 150 K.

blocking temperature of a spin glass-like phase. As the Fe content in the sample increases, the blocking temperature increases [37]. However, the highest magnetization at the minimum temperature is reached by the sample with $y = 2/3$. The ac magnetic susceptibility from 2 up to 12 K was also measured for these samples (see supplementary information). A magnetic anomaly is found in the real component at the same temperature where the peak appears in the previous ZFC measurement. This anomaly has dynamic nature (i.e. depends on the frequency of the ac field), according to the spin glass-like behavior expected for systems with magnetic frustration [35]. Fig. 8(c) displays the M(H) loops for the whole series. Although none of the curves reach magnetic saturation, the samples with $y \leq 2/3$ show some hysteresis as occurred in the $Sr_2LaSnFeO_7$ ($y = 0$) compound. Moreover, the magnetization observed at 5 T is greater for the samples with Fe-Cr mixture than for the edges of this series, achieving the highest value for the sample with $y = 2/3$ in agreement with the M(T) curves of Fig. 8(b). This can be understood in terms of the competing magnetic interactions existing in the samples. According to the magnetic transitions reported for related simple perovskites [15–17], we can assume that the strength of these interactions follows the sequence: Fe^{3+}-O-Fe^{3+}> Cr^{3+}-O-Fe^{3+} ≈ Cr^{3+}-O-Cr^{3+}. For the extremes of the series ($y = 0$ and 1), the interactions are AFM but the structural disorder causes magnetic frustration and the appearance of FM correlations which are stronger in the Fe-based sample. For intermediate compositions, the occurrence of Cr^{3+}-O-Fe^{3+} FM interactions increase the magnetization value at 5 T, being maximum for $y = 2/3$ where the distribution of a Cr surrounded by 2 Fe should be more frequent. Still, these interactions are conditioned by structural disorder and long-range order is never achieved. Our results suggest that the magnetic percolation threshold in this system is x_c>0.5, i.e. >50 % of magnetic cations are necessary in B sublattice to get a long-range magnetic order, in agreement with some studies on magnetic dilution of related RP phases with bilayers [12]. This should be ascribed to the laminar character of this structure that involves at least two types of magnetic interactions, weak interlayer and strong intralayer, to achieve a 3D order.

4. Conclusions

The hybrid improper ferroelectric $Sr_3Sn_2O_7$ can be doped with magnetic cations through a co-doping strategy, i.e., combining A-site doping (Sr^{2+} replaced by La^{3+}) and B-site doping (Sn^{4+} substituted with Cr^{3+}or Fe^{3+}). Single phases are obtained up to the replacement of half of the Sn atoms, otherwise competitive phases are segregated beyond that concentration. The XRD patterns of all co-doped samples can be refined in the orthorhombic crystal structure of the parent compound and the volume of the unit cell decreases isotropically as co-doping increases, following the ionic radii of the dopant atoms. In addition, the Cr- and/or Fe-doping hinders the stabilization of ferroelectric ordering near room temperature: T_{FE} decreases below room temperature upon lowering the Sn content and compositions with concentrations $x \geq 0.25$ are already paraelectric (and centrosymmetric) at room temperature.

Our investigation of the magnetic properties in $Sr_3Sn_2O_7$ with the different Cr and/or Fe doping, has concluded the absence of long-range magnetic order in all the studied compositions. This result suggests that the magnetic percolation threshold is x_c>0.5 at the B-site and that RP phases with perovskite bilayers exhibit greater similarity to 2D-RP phases (A_2BO_4) than to 3D perovskite structures when it comes to achieving long-range magnetic ordering. Our work evidences that structural disorder plays a key role in this type of layered structures. It is very likely that the presence of the non-magnetic rock-salt prevents the magnetic coherence between the perovskite bilayers with diluted magnetic atoms. We observed the appearance of short-range magnetic correlations instead, that give rise to a magnetic glassy system in samples with a high concentration of Fe or Fe/Cr mixtures. Summarizing, this work adds new experimental evidence to the challenging task of designing new magnetoelectrics by magnetic doping into hybrid improper ferroelectrics at room temperature, though the formation of multiferroic phases is possible at lower temperatures.

CRediT authorship contribution statement

J. Blasco: Writing – review & editing, Writing – original draft,

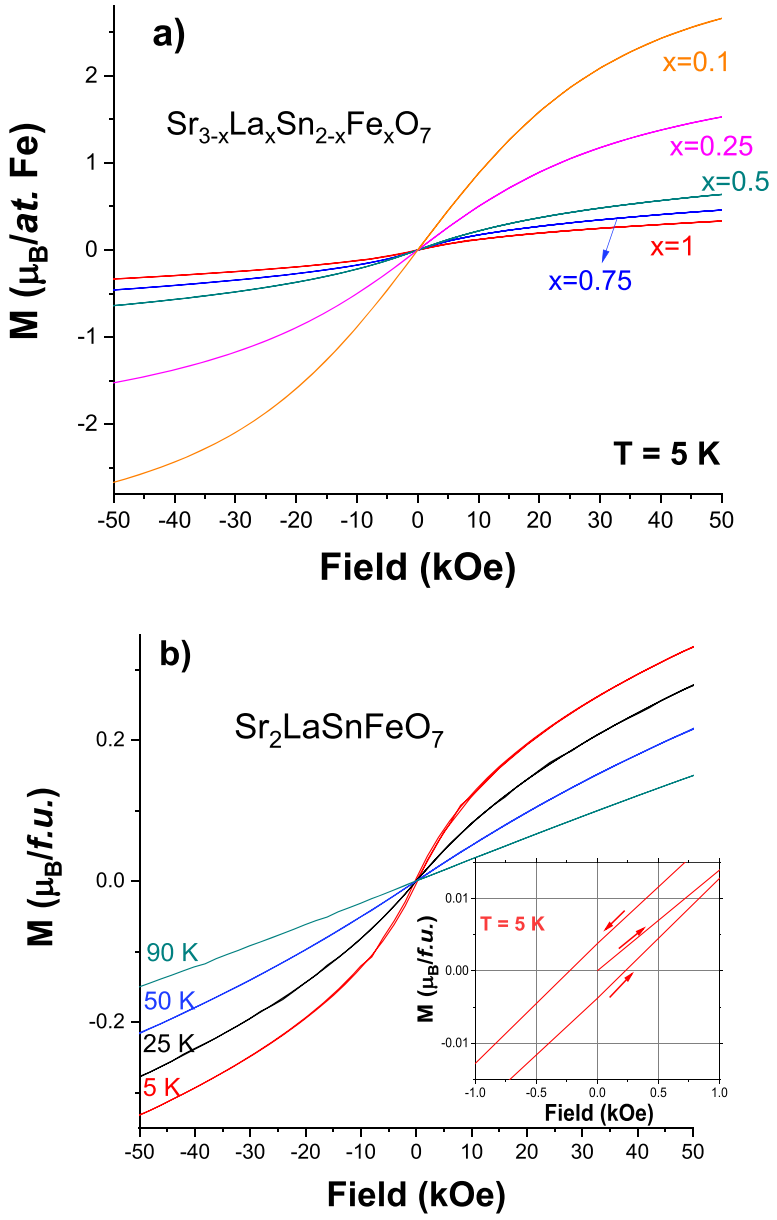

Fig. 7. (a) Magnetization loops for $Sr_{3-x}La_xSn_{2-x}Fe_xO_7$ samples at 5 K. (b) M(H) curves for $Sr_2LaSnFeO_7$ measured at selected temperatures. Inset: Detail of the M(H) measured at 5 K at very low magnetic fields.

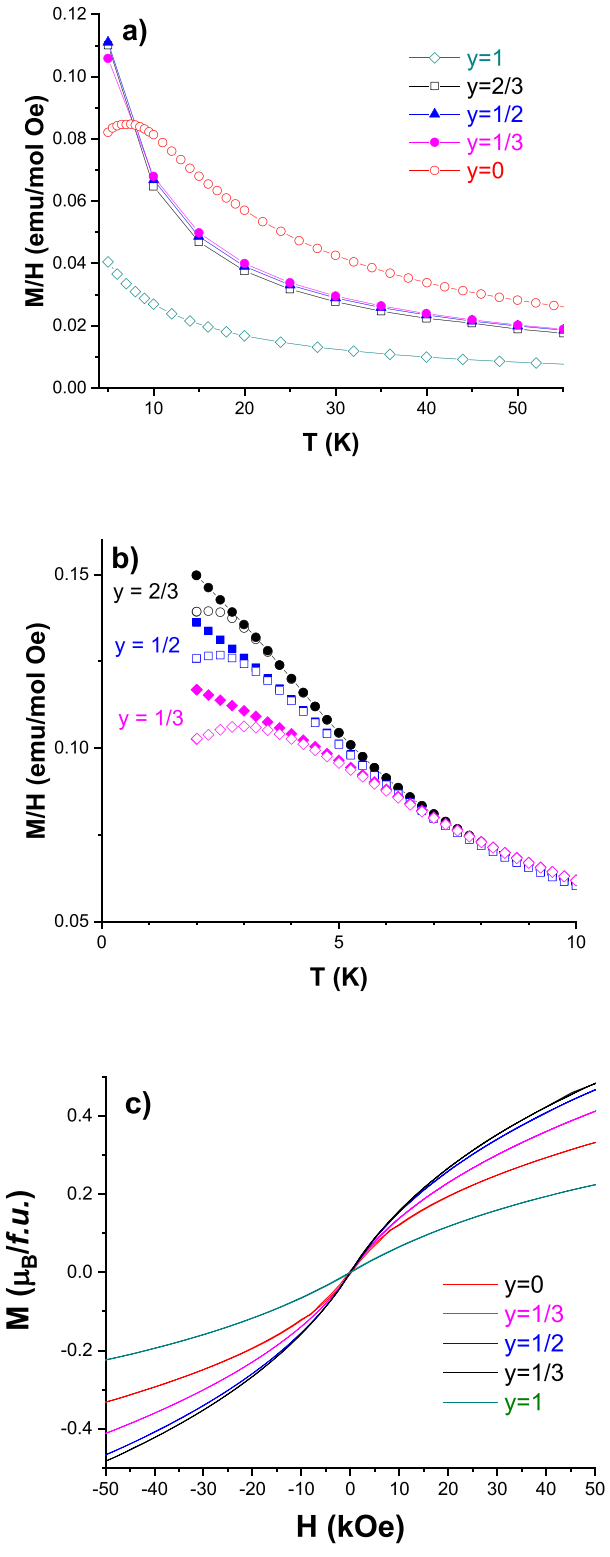

Fig. 8. (a) Magnetization vs. temperature for $Sr_2LaSnFe_{1-y}Cr_yO_7$ under an applied field of 1 kOe in zero-field conditions. (b) Detail of the M(T) curves for $Sr_2LaSnFe_{1-y}Cr_yO_7$ ($1/3 \leq y \leq 2/3$) under the same field in ZFC (open symbols) and FC conditions (dark symbols). (c) Magnetization loops for the same samples at 5 K.

Validation, Supervision, Methodology, Investigation, Formal analysis, Conceptualization. **V. Cuartero:** Writing – review & editing, Validation, Investigation, Formal analysis. **S. Lafuerza:** Writing – review & editing, Validation, Investigation, Formal analysis, Data curation. **D. Gracia:** Writing – review & editing, Validation, Investigation, Formal analysis. **J. A. Rodríguez-Velamazán:** Writing – review & editing, Investigation, Formal analysis, Data curation. **I. Puente-Orench:** Writing – review & editing, Resources, Investigation, Data curation. **G. Subías:** Writing – review & editing, Validation, Supervision, Resources, Investigation, Funding acquisition.

Declaration of competing interest

The authors declare the following financial interests/personal relationships which may be considered as potential competing interests:

Gloria Subías and Javier Blasco report that financial support was provided by the Ministry of Science and Innovation (Spain) and from the Government of Aragon (Department of Science, Technology and University). All authors declare that they have no known competing financial interests or personal relationships that could have appeared to influence the work reported in this paper.

Acknowledgements

This work has been supported by MICIU/AEI/10.13039/501100011033/FEDER, UE (PID2021-124734OB-C21, CEX2023-001286-S) and Diputación General de Aragón (E11-23R, E12-23R). D. G. acknowledges financial support from the Gobierno de Aragón through a doctoral fellowship. Authors would also like to acknowledge Servicio General de Apoyo a la Investigación from Universidad de Zaragoza. Granted beam time at ILL, via Spanish Initiatives on Neutron Scattering (SpINS), is also appreciated (Experiment CRG-2990; doi:10.5291/ILL-DATA.CRG-2990). The authors would like to express their gratitude to Dr. J. Herrero-Martín for the XAS measurement of the $Sr_2LaSnFeO_7$ sample (project number 2023027292) and ALBA synchrotron for the granted beam time.

Supplementary materials

Supplementary material associated with this article can be found, in the online version, at doi:10.1016/j.materresbull.2025.113385.

Data availability

Data will be made available on request.

References

[1] Y. Wang, F.-T. Huang, X. Luo, B. Gao, S.-W. Cheong, The first room-temperature ferroelectric Sn insulator and its polarization switching kinetics, Adv. Mater. 29 (2017) 1601288, https://doi.org/10.1002/adma.201601288.

[2] J.J. Lu, X.Q. Liu, X. Ma, M.S. Fu, A. Yuan, Y.J. Wu, X.M. Chen, Crystal structures, dielectric properties, and phase transition in hybrid improper ferroelectric $Sr_3Sn_2O_7$-based ceramics, J. Appl. Phys. 125 (2019) 044101, https://doi.org/10.1063/1.5051190.

[3] X. Xu, Y. Wang, F.-T. Huang, K. Du, E.A. Nowadnick, S.-W. Cheong, Tunable Ferroelectricity in Hybrid Improper Ferroelectric $Sr_3Sn_2O_7$, Adv. Funct. Mater. 30 (2020) 2003623, https://doi.org/10.1002/adfm.202003623.

[4] N.A. Benedek, J.M. Rondinelli, H. Djani, P. Ghosez, P. Lightfoot, Understanding ferroelectricity in layered perovskites: new ideas and insights from theory and experiments, Dalt. Trans. 44 (2015) 10543–10558, https://doi.org/10.1039/C5DT00010F.

[5] N.A. Benedek, C.J. Fennie, Hybrid Improper Ferroelectricity: A Mechanism for Controllable Polarization-Magnetization Coupling, Phys. Rev. Lett. 106 (2011) 107204, https://doi.org/10.1103/PhysRevLett.106.107204.

[6] I. Etxeberria, J.M. Pérez-Mato, P. Boullay, The Role of Trilinear Couplings in the Phase Transitions of Aurivillius Compounds, Ferroelectrics 401 (2010) 17–23, https://doi.org/10.1080/00150191003670325.

[7] R. Gupta, R.K. Kotnala, A review on current status and mechanisms of room-temperature magnetoelectric coupling in multiferroics for device applications, J. Mater. Sci. 57 (2022) 12710–12737, https://doi.org/10.1007/s10853-022-07377-4.

[8] M.F. Sykes, J.W. Essam, Critical Percolation Probabilities by Series Methods, Phys. Rev. 133 (1964) A310–A315, https://doi.org/10.1103/PhysRev.133.A310.

[9] D.J. Breed, K. Gilijamse, J.W.E. Sterkenburg, A.R. Miedema, Ordering in Two- and Three-Dimensional Diluted Heisenberg Antiferromagnets, J. Appl. Phys. 41 (1970) 1267–1268, https://doi.org/10.1063/1.1658906.
[10] S.-W. Cheong, A.S. Cooper, L.W. Rupp, B. Batlogg, J.D. Thompson, Z. Fisk, Magnetic dilution study in La_2CuO_4. Comparison with other two-dimensional magnets, Phys. Rev. B 44 (1991) 9739–9742, https://doi.org/10.1103/PhysRevB.44.9739.
[11] P.D. Battle, M.A. Green, N.S. Laskey, J.E. Millburn, L. Murphy, M.J. Rosseinsky, S. P. Sullivan, J.F. Vente, Layered Ruddlesden−Popper Manganese Oxides: Synthesis and Cation Ordering, Chem. Mat. 9 (1997) 552–559, https://doi.org/10.1021/cm960398r.
[12] S. Nair, A. Banerjee, Dilution of two-dimensional antiferromagnetism by Mn site substitution in $LaSr_2Mn_{2-x}Al_xO_7$, Phys. Rev. B 70 (2004) 104428, https://doi.org/10.1103/PhysRevB.70.104428.
[13] J.B. Goodenough, An Interpretation of the Magnetic Properties of the Perovskite Type Mixed Crystals $La_{1-x}Sr_xCoO_{3+\lambda}$, J. Phys. Chem. Solids 6 (1958) 287–297, https://doi.org/10.1016/0022-3697(58)90107-0.
[14] J. Kanamori, Superexchange interaction and symmetry properties of electron orbitals, J. Phys. Chem. Solids 10 (1959) 87–98, https://doi.org/10.1016/0022-3697(59)90061-7.
[15] G. Hearne, M.P. Pasternak, R.D. Taylor, P. Lacorre, Electronic structure and magnetic properties of $LaFeO_3$ at high pressure, Phys. Rev. B 51 (1995) 11495–11500, https://doi.org/10.1103/PhysRevB.51.11495.
[16] H. Hayashi, M. Watanabe, H. Inaba, Measurement of thermal expansion coefficient of $LaCrO_3$, Thermochim. Acta 359 (2000) 77–85, https://doi.org/10.1016/S0040-6031(00)00507-4.
[17] A.K. Azad, A. Mellergard, S.-G. Eriksson, S.A. Ivanov, S.M. Yunus, F. Lindberg, G. Svensson, R. Mathieu, Structural and magnetic properties of LaFe0.5Cr0.5O3 studied by neutron diffraction, electron diffraction and magnetometry, Mat. Res. Bull. 40 (2005) 1633–1644, https://doi.org/10.1016/j.materresbull.2005.07.007.
[18] A.P.G. Rodrigues, M.A. Morales, R.B. Silva, D.R.A.B. Lima, R.L.B.A. Medeiros, J. H. Araújo, D.M.A. Melo, Positive exchange bias effect in LaCr0.5Fe0.5O3 perovskite, J. Phys. Chem. Sol. 141 (2020) 109334, https://doi.org/10.1016/j.jpcs.2020.109334.
[19] A. Paul Blessington Selvadurai, V. Pazhanivelu, K. Suriakarthi, K. Madhan, M.-Sadeeq (Jie Tang) Balogun, R. Murugaraj, C. Venkateswaran, Ionic radii correlative study on LaFe0.5Cr0.5O3 and YbFe0.5Cr0.5O3 magnetic double perovskites, Phys. B 607 (2021) 412717, https://doi.org/10.1016/j.physb.2020.412717.
[20] S. Tiwari, M.L. Van de Put, B. Sorée, W.G. Vandenberghe, Critical behavior of the ferromagnets CrI3, CrBr3, and CrGeTe3 and the antiferromagnet FeCl2: A detailed first-principles study, Phys. Rev. B 103 (2021) 014432, https://doi.org/10.1103/PhysRevB.103.014432.
[21] H.J. Xiang, E.J. Kan, S.-H. Wei, M.-H. Whangbo, J. Yang, Origin of the Ising ferrimagnetism and spin-charge coupling in $LuFe_2O_4$, Phys. Rev. B 80 (2009) 132408, https://doi.org/10.1103/PhysRevB.80.132408.
[22] S. Lafuerza, D. Gracia, J. Blasco, M. Evangelisti, Electrocaloric effect near room temperature in lead-free Aurivillius phase Sr2Bi4Ti5O18 upon La and Nb codoping, J. Alloys Comp. 983 (2024) 173923, https://doi.org/10.1016/j.jallcom.2024.173923.
[23] B.H. Chen, T.L. Sun, X.Q. Liu, X.L. Zhu, H. Tian, X.M. Chen, Enhanced hybrid improper ferroelectricity in $Sr_{3-x}Ba_xSn_2O_7$ ceramics with a Ruddlesden–Popper (R–P) structure, Appl. Phys. Lett. 116 (2020) 04290, https://doi.org/10.1063/1.5138672.
[24] X. Sun, Z. Tang, X. Yang, Z. Gao, Y. Wu, J. Jiang, Z. Zhang, S. Jiao, D. Li, H.-L. Cai, X.S. Wu, Structural evolution and phase transition of $Sr_3Sn_2O_7$ doped with Ca, Chem. Phys. Lett. 766 (2021) 138319, https://doi.org/10.1016/j.cplett.2021.138319.
[25] J. Blasco, D. Gracia, S. Lafuerza, V. Cuartero, G. Subías, Effects of doping with magnetic cations on the hybrid improper ferroelectricity in $Sr_3Sn_2O_7$, J. Alloys Comp. 1005 (2024) 176148, https://doi.org/10.1016/j.jallcom.2024.176148.
[26] J. Rodríguez-Carvajal, Recent Advances in Magnetic Structure Determination by Neutron Powder Diffraction, Physica B 192 (1993) 55–69, https://doi.org/10.1016/0921-4526(93)90108-I.
[27] K. Momma, F. Izumi, VESTA3 for three-dimensional visualization of crystal, volumetric and morphology data, J. Appl. Crystallogr. 44 (2011) 1272–1276, https://doi.org/10.1107/S0021889811038970.
[28] A. Barla, J. Nicolas, D. Cocco, S.M. Valvidares, J. Herrero-Martín, P. Gargiani, J. Moldes, C. Ruget, E. Pellegrin, S. Ferrer, Design and performance of BOREAS, the beamline for resonant X-ray absorption and scattering experiments at the ALBA synchrotron light source, J. Synchrotron Rad. 23 (2016) 1507–1517, https://doi.org/10.1107/S1600577516013461.
[29] R.D. Shannon, Revised Effective Ionic Radii and Systematic Studies of Interatomic Distances in Halides and Chalcogenides, Acta Cryst. A 23 (1976) 751–767, https://doi.org/10.1107/S0567739476001551.
[30] S. Yoshida, H. Akamatsu, R. Tsuji, O. Hernandez, H. Padmanabhan, A.S. Gupta, A. S. Gibbs, K. Mibu, S. Murai, J.M. Rondinelli, V. Gopalan, K. Tanaka, K. Fujita, Hybrid Improper Ferroelectricity in (Sr,Ca)3Sn2O7 and Beyond: Universal Relationship between Ferroelectric Transition Temperature and Tolerance Factor in n = 2 Ruddlesden−Popper Phases, J. Am. Chem. Soc. 140 (2018) 15690–15700, https://doi.org/10.1021/jacs.8b07998.
[31] A.J. Joseph, B. Kumar, Study of true-remanent polarization using remanent hysteresis task and resistive leakage analysis in ferroelectric 0.64Pb(Mg1/3Nb2/3)O3-0.36PbTiO3 ceramics, Sol. State Comm. 271 (2018) 11–15, https://doi.org/10.1016/j.ssc.2017.12.017.
[32] Y. Zhang, J. Wang, P. Ghosez, Unraveling the Suppression of Oxygen Octahedra Rotations in $A_3B_2O_7$ Ruddlesden-Popper Compounds: Engineering Multiferroicity and Beyond, Phys. Rev. Lett. 125 (2020) 15761, https://doi.org/10.1103/PhysRevLett.125.157601.
[33] J.M.D. Coey, Magnetism and Magnetic Materials, Cambridge University Press., 2010, p. 115.
[34] F.M.F. de Groot, P. Glatzel, U. Bergmann, P.A. van Aken, R.A. Barrea, S. Klemme, M. Ha1vecker, A. Knop-Gericke, W.M. Heijboer, B.M. Weckhuysen, 1s2p Resonant Inelastic X-ray Scattering of Iron Oxides, J. Phys. Chem. B 109 (2005) 20751–20762, https://doi.org/10.1021/jp054006s.
[35] C.Y. Huang, Some experimental aspects of spin glasses: A review, J. Magn. Magn. Mat. 51 (1985) 1–74, https://doi.org/10.1016/0304-8853(85)90002-2.
[36] E. Sadrollahi, F.J. Litterst, L. Prodan, V. Tsurkan, A. Loidl, Magnetism of $CuCr_2X_4$ (X=S and Se) spinels studied with muon spin rotation and relaxation, Phys. Rev. B 110 (2024) 054439, https://doi.org/10.1103/PhysRevB.110.054439.
[37] J.A. Mydosh, Spin glasses: redux: an updated experimental/materials survey, Rep. Prog. Phys. 78 (2015) 052501, https://doi.org/10.1088/0034-4885/78/5/052501.